Quantitative Optical Coherence Tomography Angiography of Choroidal Neovascularization in Age-Related Macular Degeneration

Yali Jia, PhD,[1] Steven T. Bailey, MD,[1] David J. Wilson, MD,[1] Ou Tan, PhD,[1] Michael L. Klein, MD,[1] Christina J. Flaxel, MD,[1] Benjamin Potsaid, PhD,[2,3] Jonathan J. Liu, MS,[2] Chen D. Lu, MS,[2] Martin F. Kraus, MS,[2,4] James G. Fujimoto, PhD,[2] David Huang, MD, PhD[1]

Purpose: To detect and quantify choroidal neovascularization (CNV) in patients with age-related macular degeneration (AMD) using optical coherence tomography (OCT) angiography.

Design: Observational, cross-sectional study.

Participants: A total of 5 normal subjects and 5 subjects with neovascular AMD were included.

Methods: A total of 5 eyes with neovascular AMD and 5 normal age-matched controls were scanned by a high-speed (100 000 A-scans/seconds) 1050-nm wavelength swept-source OCT. The macular angiography scan covered a 3×3-mm area and comprised 200×200×8 A-scans acquired in 3.5 seconds. Flow was detected using the split-spectrum amplitude-decorrelation angiography (SSADA) algorithm. Motion artifacts were removed by 3-dimensional (3D) orthogonal registration and merging of 4 scans. The 3D angiography was segmented into 3 layers: inner retina (to show retinal vasculature), outer retina (to identify CNV), and choroid. En face maximum projection was used to obtain 2-dimensional angiograms from the 3 layers. The CNV area and flow index were computed from the en face OCT angiogram of the outer retinal layer. Flow (decorrelation) and structural data were combined in composite color angiograms for both en face and cross-sectional views.

Main Outcome Measures: The CNV angiogram, CNV area, and CNV flow index.

Results: En face OCT angiograms of CNV showed sizes and locations that were confirmed by fluorescein angiography (FA). Optical coherence tomography angiography provided more distinct vascular network patterns that were less obscured by subretinal hemorrhage. The en face angiograms also showed areas of reduced choroidal flow adjacent to the CNV in all cases and significantly reduced retinal flow in 1 case. Cross-sectional angiograms were used to visualize CNV location relative to the retinal pigment epithelium and Bruch's layer and classify type I and type II CNV. A feeder vessel could be identified in 1 case. Higher flow indexes were associated with larger CNV and type II CNV.

Conclusions: Optical coherence tomography angiography provides depth-resolved information and detailed images of CNV in neovascular AMD. Quantitative information regarding CNV flow and area can be obtained. Further studies are needed to assess the role of quantitative OCT angiography in the evaluation and treatment of neovascular AMD. *Ophthalmology 2014;121:1435-1444 © 2014 by the American Academy of Ophthalmology.*

Supplemental material is available at www.aaojournal.org.

Age-related macular degeneration (AMD) is the leading cause of blindness in older adults of European descent.[1] Neovascular AMD is an advanced form of macular degeneration that historically has accounted for the majority of vision loss related to AMD.[2] It is characterized by the presence of choroidal neovascularization (CNV) consisting of abnormal blood vessels that originate from the choroid. The vessels grow through Bruch's membrane (BM) and extend into the sub-retinal pigment epithelial (RPE) or subretinal space. Choroidal neovascularization can result in hemorrhage, fluid exudation, and fibrosis, resulting in photoreceptor damage and vision loss.[3] To diagnose neovascular AMD and evaluate the efficacy of treatment, determination of the presence and precise location of the CNV lesion is essential.

Fluorescein angiography (FA) and indocyanine green angiography (ICGA) are important diagnostic tools used to detect and evaluate CNV in clinical practice. Leakage of dye in the later frames of the angiogram is used to identify the presence of the CNV. Both FA and ICGA require intravenous dye injection, which can result in nausea and, rarely, anaphylaxis.[4,5]

Optical coherence tomography (OCT) generates cross-sectional images by measuring the echo time delay and magnitude of backscattered light.[6] Optical coherence tomography has achieved micrometer-level axial resolution in cross-sectional retinal imaging. The earliest retinal OCT imaging for studying neovascular AMD was based on first-generation time-domain OCT technology, which has limited speed and sensitivity.[7–9] Spectral-domain OCT has greatly

improved speed and sensitivity and is able to detect small changes in the morphology of the retinal layers and CNV activity in neovascular AMD.[10,11] More recently, swept-source OCT has demonstrated improved ranging depth by using a rapidly tuned laser and a longer wavelength (1050-nm spectral range) allowing for improved imaging beneath the RPE.[12] Therefore, this novel OCT modality is under study and may allow for better visualization of the CNV beneath the RPE.

Structural OCT, using any technology, is only sensitive to backscattering light intensity and cannot detect blood flow information. Because of this limitation, structural OCT cannot reliably discriminate vascular tissue from the surrounding tissues; thus, the precise location and activity of the CNV cannot be determined. Since 2007, several phase-based (e.g., Doppler shift,[13,14] Doppler variance,[15–17] and phase-variance[18,19]) and intensity-based (e.g., speckle variance[20–22] and decorrelation[23,24]) OCT angiography methods have been described for 3-dimensional (3D) noninvasive vasculature mapping at the microcirculation level. Miura et al[25] and Hong et al[26] recently demonstrated Doppler optical coherence angiography for imaging 3D views of ocular vascular pathology in polypoidal choroidal vasculopathy and exudative macular diseases, respectively.

Our group recently developed the split-spectrum amplitude-decorrelation angiography (SSADA) algorithm to improve the signal-to-noise ratio of flow detection.[27] This technique enables OCT angiography within a practical image acquisition time (few seconds) using a prototype that is only slightly faster than the newest generation of commercial systems. We have performed the first clinical study for demonstrating ocular vascular disturbances in glaucoma.[28]

In this study, we used OCT angiography with the SSADA algorithm[27] to investigate CNV associated with neovascular AMD. A descriptive case series of neovascular AMD is presented to describe the usefulness of OCT angiography for visualizing 3D vascular architecture and quantifying the blood flow within CNV.

Methods

Study Population

Patients were selected from clinical retina practices at the Casey Eye Institute. Patients diagnosed with neovascular AMD underwent a comprehensive eye examination and routine diagnostic evaluation consisting of color fundus photography, FA, and OCT (Spectralis; Heidelberg Engineering, Heidelberg, Germany). Inclusion criteria were patients aged more than 50 years with the presence of drusen and treatment-naïve CNV confirmed by fluorescein dye leakage on angiogram and the presence of 1 of the following on OCT: subretinal fluid, intraretinal fluid, or sub-RPE fluid. Exclusion criteria included subretinal hemorrhage >50% of the CNV lesion, visual acuity <20/200, and media opacity interfering with OCT image quality, such as cataract.

The OCT angiograms of normal subjects (aged 40−79 years) from a separate study, the Functional and Structural Optical Coherence Tomography for Glaucoma, were used as controls in this study. Inclusion criteria from that study included vision >20/40, no ocular surgery other than previous cataract surgery, and no eye disease affecting vision. As described next, 24 normal control subjects' images were used for normative retinal thickness measurements, and 5 control subjects (aged >60 years) underwent OCT angiography processing.

Patients were enrolled after informed consent in accordance with an Institutional Review Board/Ethics Committee−approved protocol at Oregon Health & Science University and in compliance with the Declaration of Helsinki. Once consent was obtained, patients underwent scanning with the prototype OCT system.

Optical Coherence Tomography Angiography

The prototype high-speed swept-source OCT system was built by the Laser Medicine and Medical Imaging Group at the Massachusetts Institute of Technology and followed the configuration published by Potsaid et al.[29] The device operated at an axial scan speed of 100 kHz using a swept-source cavity laser operating at 1050 nm with a tuning range of 100 nm. A resolution of 5.3 μm axially and 18 μm laterally at an imaging depth of 2.9 mm in tissue was achieved. The ocular light power exposure was 1.9 mW, which was within the American National Standards Institute safety limit.[30]

A 3×3-mm scanning area centered on the fovea was captured for blood flow measurements. In the fast transverse scanning direction, 200 axial scans were sampled along a 3-mm region to obtain a single B-scan. Eight consecutive B-scans (M-B frames) were captured at a fixed position before proceeding to the next sampling location. A total of 200 locations along a 3-mm region in the slow transverse direction were sampled to form a 3D data cube. With a B-scan frame rate of 455 frames per second, the 1600 B-scans in each scan were acquired in approximately 3.5 seconds. Four volumetric raster scans, including 2 horizontal priority fast transverse (x-fast) scans and 2 vertical priority fast transverse (y-fast) scans, were obtained consecutively in 1 session.

The SSADA algorithm was used to distinguish blood flow from static tissue as described in detail by in a previous published paper[27] and is briefly reviewed next. As seen in real-time OCT structural images, the amplitude of the signal returning from nonstatic tissue varies rapidly over time. By calculating the decorrelation of signal amplitude from consecutive B-scans, a contrast between static and nonstatic tissue is created that allows for the visualization of blood flow. However, decorrelation also can be generated by bulk (non-flow) eye motion. The SSADA algorithm was developed to minimize bulk axial motion noise due to orbital pulsation by splitting the spectrum and thereby lengthening the axial resolution element. In addition, the algorithm incorporated 3 steps to further remove motion artifacts within each angiography scan. First, using outlier analysis, the decorrelation frames with excessive median decorrelation values (i.e., frames corrupted by saccadic and micro-saccadic eye movements) were removed at each M-B scan position, and the remaining individual frames were averaged to obtain the final average decorrelation flow image. Second, if the number of remaining individual frames is less than 3 for averaging, the average decorrelation image at this location is replaced by the spatial neighbors. Third, the median decorrelation (an estimate of bulk motion effect) was calculated for each average decorrelation frame and then subtracted from it. This sets the decorrelation value for bulk tissue to approximately zero.

Physical flow phantom calibration experiments have been performed by our research group[31] and Liu et al.[32] Decorrelation can be considered as a metric for measuring fluctuation in the backscattered OCT signal amplitude (intensity) that does not depend on the average signal level. To be specific, the blood flow results in fluctuation in the amplitude of OCT fringes (speckle) as red blood cells move within a particular voxel. Thus, the 8 M-B frames contain fluctuating values of OCT output intensities at any given voxel in the flow of blood, and

the definition of decorrelation is constructed so that fluctuating intensities yield high decorrelation values (approaching 1.0). Pixels in the M-B frames that represent static tissue have constant intensities, and thus yield small decorrelation values (approaching 0). The faster that blood particles move across the laser beam, the higher is the decorrelation of the received signals within a velocity range set by the scan parameters. In other words, decorrelation is approximately linear to flow velocity (the distance traveled by red blood cells flowing across the light beam within a unit time).[31,32] However, beyond a saturation velocity that is defined by the time interval between consecutive OCT M-B frames, the decorrelation increases more slowly with velocity and eventually reaches an upper boundary.[32] This saturation velocity should be approximately 0.3 to 0.7 mm/second according to our[31] and Liu et al's[32] physical phantom experiments, accounting for our wavelength of 1050 nm and inter−M-B frame interval of 2 milliseconds. The minimum velocity is approximately 0.02 mm/second according to our phantom calibration. This is determined by the threshold decorrelation value 0.09, which is 2 standard deviations above the mean decorrelation value in the noise region, the central foveal avascular zone in normal eyes.

Motion artifacts were further corrected by applying an image registration algorithm that registered 4 orthogonal raster scanned volumes.[33] Motion correction was first performed on the structural OCT data. The motion correction algorithm generated 3D displacement fields that map A-scans from the input volumes into a common motion-corrected space. The same displacement fields were applied to the decorrelation (flow) data to produce motion-corrected flow data volumes. Flow data from 4 input volumes were weighted and merged,[33] improving the signal-to-noise ratio in the flow signal and reducing the flow measurement variation due to local flow changes caused by the cardiac cycle.

To enhance visualization, the 3D angiogram was separately projected into en face views (Fig 1, available at www.aaojournal.org) in 3 layers using an automated algorithm.[34,35] The inner retinal layer was defined from the internal limiting membrane to the outer boundary of the outer plexiform layer (OPL). Thus defined, the inner retina should contain all of the normal retinal vasculature. The outer retinal layer was defined from the outer OPL to the BM. Because the outer retina is normally avascular, any flow in this layer could be interpreted as CNV. The choroidal layer was defined as below BM. All of these boundaries were identified through the analysis of the reflectance and reflectance-gradient profiles in depth. Clinician's interpretation and manual identification of BM and the OPL was necessary when pathologies such as pigment epithelial detachment (PED) and intraretinal fluid obscured the outer retinal landmarks (AMD case 3). Separate en face images of the inner retina, outer retina, and choroid were presented in a sepia color scale. A composite view was developed, where each layer was assigned a different color (Figs 1−4; Figs 1 and 4, available at www.aaojournal.org) to aid with visualization as follows. The inner retina contained normal retinal circulation and was coded purple. The outer retinal layer contained any potential CNV and was coded yellow. The choroid layer was coded red.

Structural OCT features were added to OCT angiography with composite en face view and color coding demonstrating subretinal fluid (dark blue) and intraretinal cysts (light blue). These 2 types of fluid are both detected using a level-set segmentation method[36] because the reflectance of cysts and subretinal fluid is significantly lower than the surrounding tissue in the retina. On the basis of the difference among their position, shape, and size, these fluid regions can be classified as intraretinal or subretinal. In addition, the variation in retinal thickness was calculated, normalized by the normal retina thickness range, and presented

as a retinal thickness deviation map. For the purpose of this pilot study, an estimate of normal retinal thickness with the prototype OCT was obtained from 24 normal eyes from 24 subjects.

A method was developed to remove flow projection artifacts. The cross-sectional angiogram (Fig 1B, available at www.aaojournal.org) showed flow projection artifacts on the photoreceptor inner segment/outer segment boundary and RPE. The projection artifacts were due to fluctuating shadows cast by flowing blood in large inner retinal vessels that cause variation in the reflected signal in deeper layers. The signal variation was detected as a decorrelation and could not be differentiated from true flow on its own. However, these artifacts were removed from under the flow pixels in the inner retina. To remove flow projection artifacts from superficial retinal blood vessels to the outer retina, we first generated a binary large inner retinal vessel map by applying a 30×30 pixel Gaussian filter. This filter removed small inner retinal vessels and masked the outer retina flow map, thus enabling the subtraction of large vessel projections. A binary outer retinal flow map was then generated by applying a 10×10 pixel Gaussian filter to remove remaining noise and mask the outer retinal flow map again to obtain a clean map. After these artifacts were removed by the mask subtraction operation, there were no longer any flow artifacts in the normally avascular outer retina, as shown in the cross-sectional color angiogram (Fig 1C) and the en face angiogram of the outer retina (Fig 1E).

To quantify the blood flow within the CNV, the CNV area and flow index were calculated from the 2-dimensional maximum projection outer retina CNV angiogram. The CNV area was calculated by multiplying the number of pixels (for which the decorrelation value was above that of the background) and the pixel size. The CNV flow index was the average decorrelation value in the CNV region, given by,

$$\frac{\int_A D \cdot V dA}{\int_A dA} \quad (V = 1, \text{ if vessel; } V = 0, \text{ if not}),$$

where D is the decorrelation value acquired by SSADA. V is 1 when the decorrelation value was above the background; otherwise, V is 0. Flow index is a dimensionless parameter between 0 and 1 that is proportional to the density of blood vessels (fractional area occupied by vessels) and the velocity of blood flow in the CNV region.

Results

The OCT angiograms of 5 neovascular AMD eyes were compared with 5 normal eyes. The CNV area and flow index were calculated from all neovascular AMD cases. None of the 5 normal cases had flow detected in the outer retina, and CNV area and flow index were zero. A representative normal control case and 3 of the neovascular AMD cases are presented.

Normal Control Case

A 69-year-old woman with no ocular disease served as a control case (Fig 1, available at www.aaojournal.org). The inner retinal angiogram (Fig 1D) showed the normal retinal circulation with a small foveal avascular zone of approximately 0.6 mm in diameter. The absence of any flow in the outer retinal layer (Fig 1E) allowed easy detection of CNV in the cases to be shown later. The absence of blood flow in the outer retina was noted in all 5 normal control participants. The flow in the inner choroid was nearly confluent (Fig 1C, F) and masked the vascular
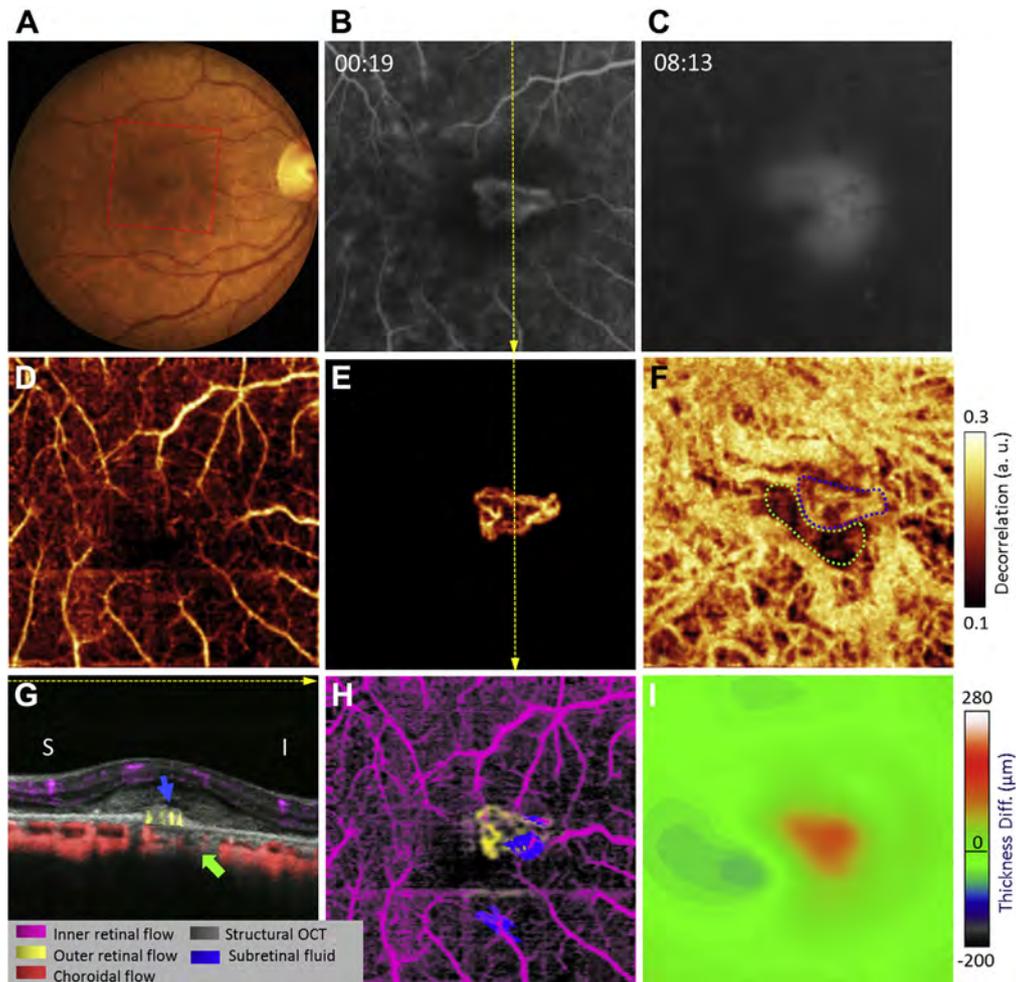
Figure 2. Case 1 with age-related macular degeneration (AMD): type I choroidal neovascularization (CNV). **A,** Color fundus photograph showing sub-retinal hemorrhage. *Red square* outlines the area shown on angiograms below. **B,** Early-phase fluorescein angiography (FA). **C,** Late-phase FA. **D,** En face optical coherence tomography (OCT) angiogram of the inner retina. **E,** En face angiogram of the outer retina showing the CNV. The *yellow dashed lines* indicate the position of OCT cross-section shown in **G**. *Yellow arrows* indicate the superior to inferior direction. **F,** En face angiogram of the choroid showing patchy flow directly under the CNV (*blue dotted outline*) and an adjacent area of reduced flow (*green dotted outline*). **G,** Cross-sectional color OCT angiogram showing the CNV (*yellow*) was predominantly under the retinal pigment epithelial (RPE). The *blue arrow* shows the location of the subretinal fluid. The *green arrow* corresponds to the *green dashed outline* in **F** showing a focal region of reduced choroidal flow adjacent to the CNV. **H,** Composite en face OCT angiograms showing most subretinal fluid (*dark blue*) inferior to the CNV. **I,** Retinal thickness deviation map showing retinal thickening over the CNV. I = inferior; S = superior.

patterns in the outer choroid and sclera in the en face angiogram (Fig 1F). The signal voids in the larger vessels in the outer choroid were due to the high flow velocity (Fig 1A−C).

Age-related Macular Degeneration Case 1

A 65-year-old woman noted vision loss in her right eye for 1 month. Visual acuity measured 20/100 in the right eye. Fundus photography (Fig 2A) showed drusen and a small subretinal hemorrhage associated with a gray subretinal lesion just nasal to the fovea. Fluorescein angiography (Fig 2B, C) revealed early hyperfluorescence with late leakage consistent with classic CNV.

Optical coherence tomography angiography showed a normal retinal circulation (Fig 2D, H). The outer retinal OCT angiogram (Fig 2E, H) showed high flow in a CNV network in a pattern strikingly similar to the early phase of FA. The cross-sectional color OCT angiogram (Fig 2G) showed the CNV to be underneath the RPE and above the BM, indicating type I CNV. The subretinal hemorrhage above the CNV (Fig 2G) did not seem to obscure the CNV on the FA or OCT angiograms (Fig 2E, H).

The en face OCT angiogram of the choroid (Fig 2F) showed loss of choriocapillaris revealing deeper, larger choroidal vessels (compare with normal choroid in Fig 1F). An area inferotemporal to the CNV had particularly low flow in both the choriocapillaris and the deeper choroid (Fig 2F, green outline). This low flow choroidal region had high OCT reflectance signal (Fig 2G, green arrow); therefore, the reduced flow was not caused by a shadow artifact.

The composite en face OCT angiogram (Fig 2H) showed that the CNV was at the superonasal edge of the fovea avascular zone (FAZ) and that subretinal fluid was accumulated next to the CNV. The OCT retinal thickness map (Fig 2I) showed retinal
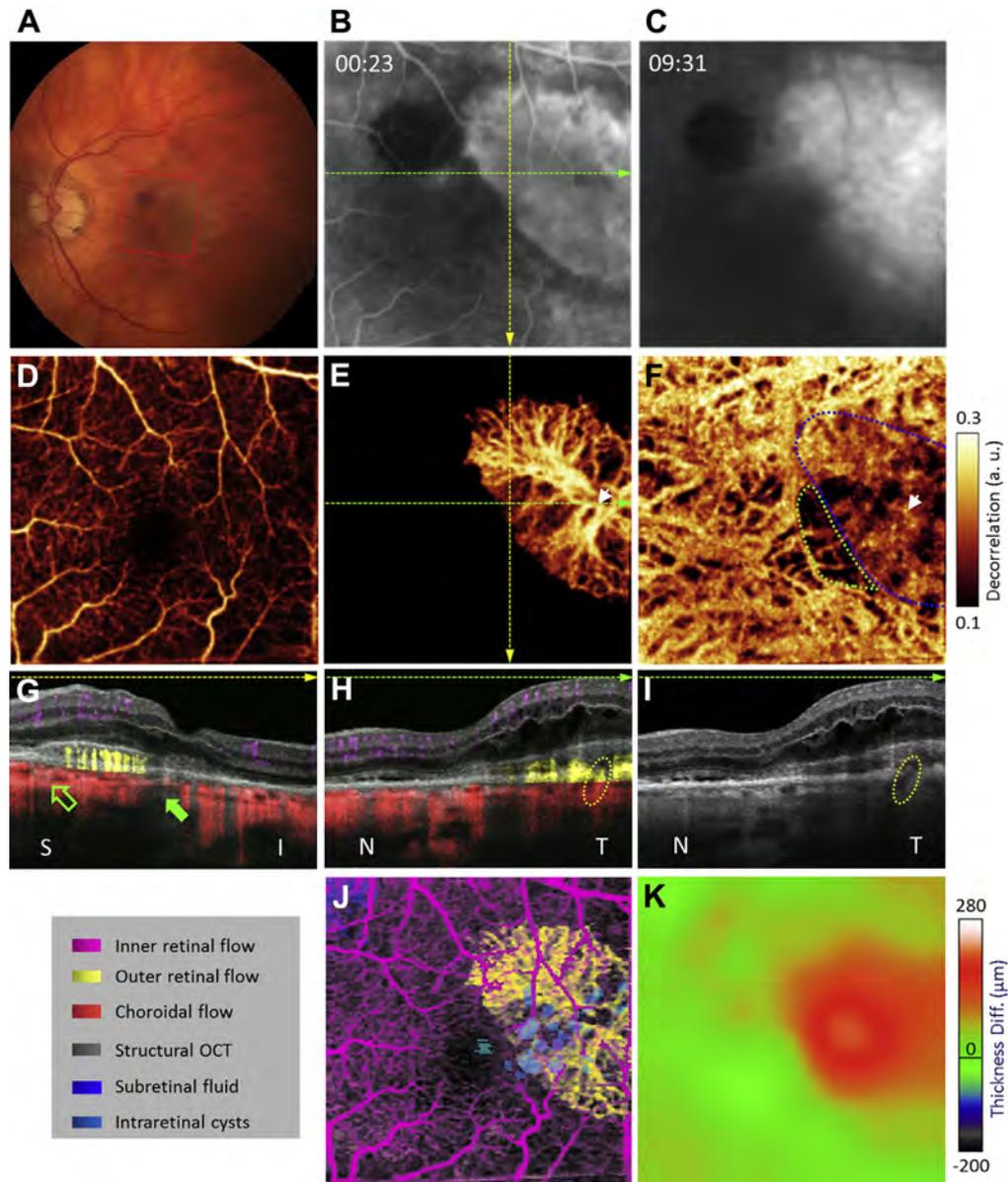
Figure 3. Case 2 with age-related macular degeneration (AMD): type II choroidal neovascularization (CNV). **A,** Fundus photography showing subretinal hemorrhage. The *red square* outlines the area shown on angiograms below. **B,** Early-phase fluorescein angiography (FA). **C,** Late-phase FA. **D,** En face optical coherence tomography (OCT) angiogram of the inner retina. **E,** En face OCT angiogram of the outer retina showing the CNV. The *yellow* and *green dashed lines* indicate the position of OCT cross-section shown in **G, H,** and **I. F,** En face angiogram of the choroid showing the patchy reduced flow directly under the CNV (*blue dotted outline*) and an adjacent area of reduced flow (*green dotted outline*). **G,** Vertical cross-sectional color OCT angiogram showing the CNV (*yellow*) was predominantly above the retinal pigment epithelial (RPE). The *green solid arrow* corresponds to the *green dotted outline* in **F** showing a focal region of reduced choroidal flow inferonasal to the CNV. The *green hollow arrow* points out a high choroidal flow signal superior to the CNV. **H,** Horizontal cross-sectional color OCT angiogram showing the feeder vessel (*yellow dotted circle*) that corresponds to the *white arrows* in **E** and **F**. Also note cystic intraretinal fluid above the CNV. **I,** Horizontal cross-sectional OCT reflectance image showing the feeder vessel seen as a flow void. **J,** Composite en face OCT angiogram showing subretinal fluid (*dark blue*) at the superonasal corner and intraretinal fluid (*light blue*) over the CNV. **K,** Retinal thickness deviation map showing thickening over the CNV. Fly-through movies of 3D color OCT angiograms are available as supplement Videos 1 and 2 (available at www.aaojournal.org).

thickening over the CNV that was primarily due to the inclusion of subretinal hemorrhage (Fig 2G) in the retinal thickness measurement and an element of retinal edema inferior to the CNV. These en face OCT views combined angiographic (CNV size, location, flow) and structural information (fluid, edema) that would be useful for clinical management.

Age-related Macular Degeneration Case 2

A 76-year-old woman noticed vision loss in her left eye for 1 week. Visual acuity measured 20/30, and fundus examination (Fig 3A) of the left eye revealed drusen and a gray/green lesion in the temporal macula with associated subretinal hemorrhage. Early frames of the

FA revealed a hyperfluorescent vascular network in the temporal macula with late leakage (Fig 3B, C).

The OCT angiography showed details of the CNV structure, with a central feeder vessel from which radiated thick core vessels ending in fine vascular fronds (Fig 3E, J; Video 1, available at www.aaojournal.org). Both the FA and OCT angiogram showed an identical CNV location, with slight notching at the superonasal edge due to shadowing from the small patch of subretinal hemorrhage. Cross-sectional OCT angiography (Fig 3G, H; Video 2, available at www.aaojournal.org) revealed that most of the CNV flow was above the RPE, indicating a predominantly type II CNV. Because of the flow projection artifact, there appeared to be flow in the RPE below the CNV.

The en face OCT angiogram of the choroid (Fig 3F) showed patchy loss of choriocapillaris, which allowed visualization of intermediate-to-large deeper choroidal vessels that were not visible in the healthy control (Fig 1F). There were focal regions under and adjacent to the CNV where there was greatly reduced flow in both the choriocapillaris and the deeper choroid (Fig 3F–H). Although some of this might be explained by shadowing under the CNV, the hypoperfused choroid adjacent to the CNV had normal OCT reflectance (Fig 3I), suggesting that the loss of choroidal flow was real rather than an artifact.

The composite en face OCT angiogram showed that the CNV was at the superotemporal edge of the FAZ. Subretinal fluid accumulated superonasal to the CNV, and intraretinal cystic fluid accumulated above the CNV. Retinal thickening shown on the relative thickness map (Fig 3K) correlated with the intraretinal fluid accumulation.

Age-related Macular Degeneration Case 3

An 88-year-old woman noted vision loss in her right eye for several months (Fig 4, available at www.aaojournal.org). Visual acuity in the right eye was 20/200. Fundus photography (Fig 4A) demonstrated chronic geographic atrophy in the superior nasal macula with new subretinal hemorrhage and an associated RPE tear temporal to the geographic atrophy. Fluorescein angiography showed late leakage consistent with a CNV (Fig 4B, C). However, the location of the CNV was unclear because of blocking from the subretinal hemorrhage. Hypofluorescence from the scrolled RPE and hyperfluorescence-associated geographic atrophy were evident.

The inner retinal angiogram in this case (Fig 4D) showed an apparent reduction in inner retinal blood flow that may have indicated retinal atrophy. This patient had difficulty with fixation, and slight motion artifacts (horizontal and vertical dark lines) were evident despite the use of 3D registration software.

The OCT angiography of the outer retina (Fig 4E–H) showed a distinct CNV adjacent to the subretinal hemorrhage. The nasal edge of the CNV was blocked from view where the subretinal hemorrhage was thicker and cast a shadow. The cross-sectional OCT angiogram (Fig 4G) revealed high CNV flow at the edge of the RPE tear. Flow was detected both above and below the RPE, indicating a combined type I and type II lesion. In addition to the CNV, there was accumulation of a large amount of stationary (nonvascular) material under the PED.

The en face choroidal angiogram (Fig 4F) showed reduced signal both under the PED and in the area of geographic atrophy. The area under the PED showed low reflectance on OCT cross-section (Fig 4G) and no vascular pattern on the en face OCT angiogram (Fig 4F). This suggested that the reduced choroidal flow was a shadow artifact associated with the PED and scrolled RPE (Fig 4F). A similar area of blocked fluorescence was present on FA (Fig 4B, C). In contrast, the area of geographic atrophy showed distinct large, deep choroidal vessels and loss of choriocapillaris.

The composite en face OCT angiogram (Fig 4H) showed the CNV to be inferior to the FAZ and associated with a surrounding accumulation of both intraretinal and subretinal fluids. There was retinal thinning over the CNV (Fig 4I), possibly due to focal compression from the highly elevated CNV and RPE tear (Fig 4G). There was gross retinal thickening around the CNV (Fig 4I) associated with fluid accumulation (Fig 4H). The heavy accumulation of intraretinal fluid and reduced retinal blood flow visualized on the en face composite OCT angiogram may explain the poor visual acuity.

Evaluation of Choroidal Flow in Age-related Macular Degeneration

The OCT angiography of the choroid showed reduced inner choroidal flow in all 5 AMD cases compared with the control cases that allowed visualization of larger and deeper choroidal vessels. Conventional FA and structural OCT did not reveal geographic atrophy or other abnormalities that accounted for the choriocapillaris atrophy in most of these areas. In addition, focal areas of decreased flow in both superficial and deeper choroidal vessels were associated with CNV in all of the AMD cases, except for case 3, in whom the presence of a focal choroidal flow defect could not be determined because of shadowing by the scrolled RPE (Fig 4F).

Quantification of the Area and Flow Index of Choroidal Neovascularization

Quantitative measurements of CNV area and flow index are summarized in Table 1. High flow index indicated active blood flow within the CNV. Higher flow was detected with larger CNVs and those that were type II compared with type I and combined CNVs.

Discussion

Structural OCT has become an indispensable tool in the management of AMD. It allows the clinician to assess fluid exudation from CNV as manifested by intraretinal cysts, retinal thickening, and subretinal fluid accumulation. It identifies the alterations in normal retinal anatomy that are associated with visual potential. However, structural OCT images cannot identify the CNV structure itself. Although structural OCT can identify abnormal tissue above or below the RPE that might be CNV, positive identification is not possible because CNV tissue has similar reflectivity as drusenoid material, hemorrhage, RPE, and choroid.[37] Therefore, FA or ICGA is still needed in the initial diagnosis of neovascular AMD. Because FA and ICGA require intravenous dye injection, nausea and vomiting are common adverse reactions, and serious anaphylactic reactions are possible.[4,5] Therefore, it is highly desirable to develop a noninvasive method of imaging CNV. Two-dimensional flow imaging technologies, such as scanning laser Doppler flowmetry,[38] laser speckle photography,[39] and laser speckle flowgraphy,[40] are not able to clearly distinguish flow in the CNV from the underlying choroidal circulation. A 3D flow imaging technology, such as OCT angiography, is needed.

Miura et al[25] and Hong et al[26] used Doppler optical angiography to image CNV associated with neovascular AMD, polypoidal vasculopathy, and myopic macular

Table 1. Summary of Choroidal Neovascularization Types, Area, and Flow Index of 5 Scanned Age-related Macular Degeneration Cases

AMD Case No.	Sex/Age	CNV Types	CNV Area (mm²)	CNV Flow Index (au)
1	Female/65 yrs	I	0.29	0.127
2	Female/76 yrs	II	2.18	0.146
3	Female/88 yrs	Combined	0.13	0.130
4	Female/85 yrs	II	0.89	0.148
5	Male/70 yrs	Combined	0.05	0.120

AMD = age-related macular degeneration; au = arbitrary unit; CNV = choroidal neovascularization.

degeneration. However, in their pioneering work, it remained difficult to distinguish the CNV from the retinal and choroidal vasculature in the en face projection views, and quantification of CNV was not attempted. In this article, we reported improvements in OCT angiography segmentation, visualization, and quantification to provide comprehensive information that a clinician could use to assess and manage CNV.

We investigated the capability of OCT angiography for imaging and quantifying CNV in patients with neovascular AMD. A high-speed swept-source OCT system at 1050 nm wavelength provided for deeper penetration compared with standard 830 nm OCT and improved imaging below the RPE. We used a new type of OCT angiography algorithm called "SSADA," which is based on detecting the reflectance amplitude (or intensity) variation over time due to flow in vascular volumes. Neither amplitude- nor intensity-based OCT angiography requires accurate determination of background tissue phase variation due to motion, and are therefore more robust than Doppler or phase-based OCT angiography.[31] The SSADA algorithm improves on the standard amplitude or intensity-based algorithms[20,22,23,41] by enhancing signal and suppressing noise through spectral splitting of the OCT images.[27]

We segmented the 3D angiograms into 3 separate vascular layers. By taking advantage of the fact that the outer retinal layer is normally devoid of blood flow, we were able to provide clean en face visualization of the CNV structure. By optimizing the choice of color and transparency, we were able to highlight the CNV relative to the inner retinal vascular pattern in a composite en face angiogram. Evidence of CNV activity, such as subretinal fluid and intraretinal cysts, was also incorporated into the composite view. This may be helpful to the clinician in the rapid assessment of CNV and its response to treatment. Because both functional (blood flow) and structural (fluid accumulations) information are taken from a single OCT scan, they are naturally perfectly registered. This is simpler and potentially faster and more robust than combining structural OCT with FA or ICGA taken from separate instruments.

By using these new imaging, processing, and display technologies, we successfully identified blood flow in CNVs in 5 treatment-naïve neovascular AMD cases. The SSADA flow signal was useful in distinguishing CNV from the surrounding outer retinal tissue, hemorrhage, RPE, BM, and

nonflow material under PEDs. By using color OCT cross-sectional angiograms that combined flow and structural information, we were able to determine the position of the CNV relative to the RPE and BM, and thereby classify the CNV as type I, type II, or combined type. In 1 case, a feeder vessel between the choroid and the CNV was successfully visualized (Fig 3), which is rarely possible using FA and ICGA. The position of the CNV on en face OCT images was confirmed by FA in all 5 cases. Compared with FA, en face OCT angiograms show a more distinct CNV vascular network pattern that is less obscured by overlying subretinal hemorrhage, as one would expect because of the longer wavelength used by OCT.

Our pilot study also demonstrated, for the first time, quantitative assessments of CNV area and flow index that are proportional to average avascular density and flow velocity on the capillary scale. In our small sample of 5 patients, we noticed that higher CNV flow was associated with larger CNV area and type II classification, but larger studies are needed to confirm these associations. Measurements of CNV area and flow index provide new information on CNV activity that may be early indicators of treatment response or relapse. Further studies are needed to assess the clinical utility of these new image-derived metrics.

In addition to providing depth-resolved information of CNV, OCT angiography may provide further insight into choroidal flow and AMD pathogenesis. En face choroidal angiograms of the control cases showed confluent signals from choriocapillaris that obscured visualization of larger, deeper choroidal vessels. In all 5 of the AMD cases, deep choroidal vessels were more apparent, and we suspect this is due to loss of choriocapillaris associated with AMD. Some regions of choriocapillaris loss could be due to geographic atrophy (Fig 4F) or shadowing from thick hemorrhage, CNV, or PED. However, there were also areas of choriocapillaris loss that could not be attributed to geographic atrophy or shadowing effect. Particularly notable among these areas were focal regions adjacent to CNV, where there was total absence of choriocapillaris with loss of both inner and deeper choroidal vessels. We suspect these focal areas of choroidal hypoperfusion with possible outer retinal ischemia may have a role in CNV pathogenesis. Studies[42,43] have identified abnormalities in choroidal flow associated with CNV in AMD. McLeod et al[44] provided histologic evidence of choriocapillaris atrophy in the vicinity of CNV. Although ICGA has often been used to assess the choroidal circulation in CNV, the noninvasive nature of OCT angiography may allow for more frequent assessments of choroidal changes in large, longitudinal clinical studies to identify possible precursors to neovascular AMD development.

In addition to its noninvasive nature, OCT angiography has several compelling characteristics that make it a promising modality for clinical use. Optical coherence tomography angiography can be acquired in a few seconds, compared with several minutes for FA. The 3D imaging allows for depth resolution of pathology and separation of individual vascular layers for evaluation. The OCT angiography scan pattern and SSADA processing can be implemented on spectral-domain or swept-source OCT systems without any special hardware modification.

In addition, the new SSADA algorithm allows for relatively quantitative reliable flow measurements. By using decorrelation instead of variance of reflected signal to measure flow, the measurement is largely independent of OCT signal strength level over a wide range.[28,45] This is important because previous techniques, such as laser Doppler flowmetry (e.g., Heidelberg Retinal Flowmeter, Heidelberg Engineering), could not reliably compare flow values between individuals because of the effect of signal strength on the measurements.[46–50] In the SSADA algorithm, background bulk tissue motion was measured and removed at 3 different levels (see "Methods"). This was highly effective as demonstrated by the absence of any retinal flow in normal subjects in the foveal avascular zone and in the outer retina in general. Thus, the flow index is a relatively clean measure of blood flow. Another strength of SSADA is that the decorrelation measures flow in both transverse and axial directions with nearly equal sensitivity. This omnidirectional nature has been verified experimentally.[31] This is different from Doppler shift-based techniques,[13,14] which are more sensitive to axial flow than transverse flow. Chorioretinal vessels are largely transverse to the OCT probe beam, but vary over a range of incidence angles. Doppler shift-based flow measurements are biased by incidence angle, unless the Doppler angle is explicitly measured[51,52] or otherwise accounted for.[53–56] The decorrelation value measured by SSADA is independent of incident angle and therefore a more robust measurement of flow. Certainly, a limitation of decorrelation and its derived flow indexes is that they are in arbitrary units and affected by imaging parameters, such as the time interval among consecutive B-scan (cross-sectional) image frames, split-spectral bandwidth, and the wavelength. The spot diameter also may have an effect. However, because these parameters are fixed for OCT systems or can be controlled by software, it is possible to keep these parameters constant and make meaningful measurement that could be compared between individuals and between visits.

Study Limitations

There are several limitations to OCT angiography. High scanning speed is needed to provide sufficient cross-sectional frame rate to overcome background eye motion. Therefore, the current generation of commercial OCT systems at 20 to 40 kHz speed may be insufficient. The next generation of OCT systems, running at 70 to 100 kHz, is likely required. In the present study, the 100 kHz OCT prototype image provided a small 3-mm square field of view. We have recently improved the scan and processing software to provide a 4-mm field of view. However, a larger field of view will require an even higher speed. Because laboratory OCT prototypes of multi-MHz speed have been reported,[57–59] we believe the speed and scan size area limitations will be solved as commercial implementation catches up to laboratory technology. Fluorescein angiography provides dynamic information currently not available with OCT angiography, such as transit time of fluorescein dye to travel to the eye. In addition, changes in patterns of fluorescence over time (staining, leakage, pooling) are used

for identifying and distinguishing various pathologic conditions, as well as assessing disease activity, such as CNV. Flow detected on OCT angiography alone will not account for all of this information. However, it is possible in the future that combining information from OCT, such as fluid identified with structural OCT, segmentation of individual structures such as RPE (providing information analogous to staining), and angiographic OCT flow information, may allow for more comprehensive clinical picture with OCT technology.

In conclusion, this pilot study demonstrated the ability of OCT angiography, with the SSADA algorithm, to image CNV and provide quantitative data in its natural state. Additional studies evaluating change in CNV structure, CNV area, and flow index while under treatment with anti-vascular endothelial growth factor therapy are under way. We hope future investigations of quantitative OCT angiography will aid with the evaluation and management of neovascular AMD.

References

1. Eye Diseases Prevalence Research Group. Causes and prevalence of visual impairment among adults in the United States. Arch Ophthalmol 2004;122:477–85.
2. Ferris FL III, Fine SL, Hyman L. Age-related macular degeneration and blindness due to neovascular maculopathy. Arch Ophthalmol 1984;102:1640–2.
3. Ambati J, Ambati BK, Yoo SH, et al. Age-related macular degeneration: etiology, pathogenesis, and therapeutic strategies. Surv Ophthalmol 2003;48:257–93.
4. Stanga PE, Lim JI, Hamilton P. Indocyanine green angiography in chorioretinal diseases: indications and interpretation: an evidence-based update. Ophthalmology 2003;110:15–21.
5. Lopez-Saez MP, Ordoqui E, Tornero P, et al. Fluorescein-induced allergic reaction. Ann Allergy Asthma Immunol 1998;81:428–30.
6. Huang D, Swanson EA, Lin CP, et al. Optical coherence tomography. Science 1991;254:1178–81.
7. Hee MR, Baumal CR, Puliafito CA, et al. Optical coherence tomography of age-related macular degeneration and choroidal neovascularization. Ophthalmology 1996;103:1260–70.
8. Do DV, Gower EW, Cassard SD, et al. Detection of new-onset choroidal neovascularization using optical coherence tomography: the AMD DOC Study. Ophthalmology 2012;119:771–8.
9. Coscas F, Coscas G, Souied E, et al. Optical coherence tomography identification of occult choroidal neovascularization in age-related macular degeneration. Am J Ophthalmol 2007;144:592–9.
10. Framme C, Panagakis G, Birngruber R. Effects on choroidal neovascularization after anti-VEGF upload using intravitreal ranibizumab, as determined by spectral domain-optical coherence tomography. Invest Ophthalmol Vis Sci 2010;51:1671–6.
11. Sayanagi K, Sharma S, Yamamoto T, Kaiser PK. Comparison of spectral-domain versus time-domain optical coherence tomography in management of age-related macular degeneration with ranibizumab. Ophthalmology 2009;116:947–55.
12. de Bruin DM, Burnes DL, Loewenstein J, et al. In vivo three-dimensional imaging of neovascular age-related macular degeneration using optical frequency domain imaging at 1050 nm. Invest Ophthalmol Vis Sci 2008;49:4545–52.

13. Hong YJ, Makita S, Jaillon F, et al. High-penetration swept source Doppler optical coherence angiography by fully numerical phase stabilization. Opt Express [serial online] 2012;20:2740–60. Available at: http://www.opticsinfobase.org/oe/fulltext.cfm?uri=oe-20-3-2740&id=226741. Accessed December 10, 2013.

14. Grulkowski I, Gorczynska I, Szkulmowski M, et al. Scanning protocols dedicated to smart velocity ranging in spectral OCT. Opt Express [serial online] 2009;17:23736–54. Available at: http://www.opticsinfobase.org/oe/abstract.cfm?uri=oe-17-26-23736. Accessed December 10, 2013.

15. Liu G, Qi W, Yu L, Chen Z. Real-time bulk-motion-correction free Doppler variance optical coherence tomography for choroidal capillary vasculature imaging. Opt Express [serial online] 2011;19:3657–66. Available at: http://www.opticsinfobase.org/oe/fulltext.cfm?uri=oe-19-4-3657&id=210023. Accessed December 10, 2013.

16. Wang L, Wang Y, Guo S, et al. Frequency domain phase-resolved optical Doppler and Doppler variance tomography. Opt Commun 2004;242:345–50.

17. Yu L, Chen Z. Doppler variance imaging for three-dimensional retina and choroid angiography. J Biomed Opt 2010;15:016029.

18. Fingler J, Zawadzki RJ, Werner JS, et al. Volumetric microvascular imaging of human retina using optical coherence tomography with a novel motion contrast technique. Opt Express [serial online] 2009;17:22190–200. Available at: http://www.opticsinfobase.org/oe/abstract.cfm?uri=oe-17-24-22190. Accessed December 10, 2013.

19. Kim DY, Fingler J, Werner JS, et al. In vivo volumetric imaging of human retinal circulation with phase-variance optical coherence tomography. Biomed Opt Express [serial online] 2011;2:1504–13. Available at: http://www.opticsinfobase.org/boe/fulltext.cfm?uri=boe-2-6-1504&id=213832. Accessed December 10, 2013.

20. Hendargo HC, Estrada R, Chiu SJ, et al. Automated non-rigid registration and mosaicing for robust imaging of distinct retinal capillary beds using speckle variance optical coherence tomography. Biomed Opt Express [serial online] 2013;4:803–21. Available at: http://www.opticsinfobase.org/boe/fulltext.cfm?uri=boe-4-6-803&id=253337. Accessed December 10, 2013.

21. Mariampillai A, Leung MK, Jarvi M, et al. Optimized speckle variance OCT imaging of microvasculature. Opt Lett 2010;35:1257–9.

22. Mariampillai A, Standish BA, Moriyama EH, et al. Speckle variance detection of microvasculature using swept-source optical coherence tomography. Opt Lett 2008;33:1530–2.

23. Enfield J, Jonathan E, Leahy M. In vivo imaging of the microcirculation of the volar forearm using correlation mapping optical coherence tomography (cmOCT). Biomed Opt Express [serial online] 2011;2:1184–93. Available at: http://www.opticsinfobase.org/boe/fulltext.cfm?uri=boe-2-5-1184&id=211771. Accessed December 10, 2013.

24. Jonathan E, Enfield J, Leahy MJ. Correlation mapping method for generating microcirculation morphology from optical coherence tomography (OCT) intensity images. J Biophotonics 2011;4:583–7.

25. Miura M, Makita S, Iwasaki T, Yasuno Y. Three-dimensional visualization of ocular vascular pathology by optical coherence angiography in vivo. Invest Ophthalmol Vis Sci 2011;52:2689–95.

26. Hong YJ, Miura M, Makita S, et al. Noninvasive investigation of deep vascular pathologies of exudative macular diseases by high-penetration optical coherence angiography. Invest Ophthalmol Vis Sci 2013;54:3621–31.

27. Jia Y, Tan O, Tokayer J, et al. Split-spectrum amplitude-decorrelation angiography with optical coherence tomography. Opt Express 2012;20:4710–25.

28. Jia Y, Morrison JC, Tokayer J, et al. Quantitative OCT angiography of optic nerve head blood flow. Biomed Opt Express [serial online] 2012;3:3127–37. Available at: http://www.optic-sinfobase.org/boe/fulltext.cfm?uri=boe-3-12-3127&id=245369. Accessed December 10, 2013.

29. Potsaid B, Baumann B, Huang D, et al. Ultrahigh speed 1050nm swept source/Fourier domain OCT retinal and anterior segment imaging at 100,000 to 400,000 axial scans per second. Opt Express 2010;18:20029–48.

30. American National Standard for Safe Use of Lasers, ANSI Z136. Orlando, FL: Laser Institute of America; 2007:1–2007.

31. Tokayer J, Jia Y, Dhalla AH, Huang D. Blood flow velocity quantification using split-spectrum amplitude-decorrelation angiography with optical coherence tomography. Biomed Opt Express [serial online] 2013;4:1909–24. Available at: http://www.optic-sinfobase.org/boe/fulltext.cfm?uri=boe-4-10-1909&id=260835. Accessed December 10, 2013.

32. Liu G, Lin AJ, Tromberg BJ, Chen Z. A comparison of Doppler optical coherence tomography methods. Biomed Opt Express [serial online] 2012;3:2669–80. Available at: http://www.optic-sinfobase.org/boe/fulltext.cfm?uri=boe-3-10-2669&id=242508. Accessed December 10, 2013.

33. Kraus MF, Potsaid B, Mayer MA, et al. Motion correction in optical coherence tomography volumes on a per A-scan basis using orthogonal scan patterns. Biomed Opt Express [serial online] 2012;3:1182–99. Available at: http://www.opticsin-fobase.org/boe/fulltext.cfm?uri=boe-3-6-1182&id=233031. Accessed December 10, 2013.

34. Tan O, Chopra V, Lu AT, et al. Detection of macular ganglion cell loss in glaucoma by Fourier-domain optical coherence tomography. Ophthalmology 2009;116:2305–14.

35. Tan O, Li G, Lu AT, et al. Mapping of macular substructures with optical coherence tomography for glaucoma diagnosis. Ophthalmology 2008;115:949–56.

36. Chan TF, Vese LA. Active contours without edges. IEEE Trans Image Process 2001;10:266–77.

37. Giovannini A, Amato GP, Mariotti C, Scassellati-Sforzolini B. OCT imaging of choroidal neovascularisation and its role in the determination of patients' eligibility for surgery. Br J Ophthalmol 1999;83:438–42.

38. Michelson G, Schmauss B, Langhans MJ, et al. Principle, validity, and reliability of scanning laser Doppler flowmetry. J Glaucoma 1996;5:99–105.

39. Briers JD, Fercher AF. Retinal blood-flow visualization by means of laser speckle photography. Invest Ophthalmol Vis Sci 1982;22:255–9.

40. Tamaki Y, Araie M, Kawamoto E, et al. Noncontact, two-dimensional measurement of retinal microcirculation using laser speckle phenomenon. Invest Ophthalmol Vis Sci 1994;35:3825–34.

41. Motaghiannezam R, Fraser S. Logarithmic intensity and speckle-based motion contrast methods for human retinal vasculature visualization using swept source optical coherence tomography. Biomed Opt Express [serial online] 2012;3:503–21. Available at: http://www.opticsin-fobase.org/boe/fulltext.cfm?uri=boe-3-3-503&id=227627. Accessed December 10, 2013.

42. Hayashi K, de Laey JJ. Indocyanine green angiography of choroidal neovascular membranes. Ophthalmologica 1985;190:30–9.

43. Melrose MA, Magargal LE, Goldberg RE, Annesley WH Jr. Subretinal neovascular membranes associated with choroidal nonperfusion and retinal ischemia. Ann Ophthalmol 1987;19:396–9.

44. McLeod DS, Grebe R, Bhutto I, et al. Relationship between RPE and choriocapillaris in age-related macular degeneration. Invest Ophthalmol Vis Sci 2009;50:4982–91.

45. Jia Y, Wei E, Wang X, et al. Optical coherence tomography angiography of optic disc perfusion in glaucoma. Ophthalmology 2014;121:1322–32.

46. Petrig BL, Riva CE. Optic nerve head laser Doppler flowmetry: principles and computer analysis. In: Kaiser HJ, Flammer J, Hendrickson P, eds. Ocular Blood Flow: New Insights into the Pathogenesis of Ocular Diseases. Basel, Switzerland: Karger; 1995:120–7.

47. Petrig BL, Riva CE, Hayreh SS. Laser Doppler flowmetry and optic nerve head blood flow. Am J Ophthalmol 1999;127:413–25.

48. Riva CE. Basic principles of laser Doppler flowmetry and application to the ocular circulation. Int Ophthalmol 2001;23: 183–9.

49. Jonescu-Cuypers CP, Chung HS, Kagemann L, et al. New neuroretinal rim blood flow evaluation method combining Heidelberg retina flowmetry and tomography. Br J Ophthalmol 2001;85:304–9.

50. Obeid A, Barnett N, Dougherty G, Ward G. A critical review of laser Doppler flowmetry. J Med Eng Technol 1990;14:178–81.

51. Wang Y, Bower BA, Izatt JA, et al. Retinal blood flow measurement by circumpapillary Fourier domain Doppler optical coherence tomography. J Biomed Opt 2008;13:064003.

52. Wang Y, Fawzi AA, Varma R, et al. Pilot study of optical coherence tomography measurement of retinal blood flow in retinal and optic nerve diseases. Invest Ophthalmol Vis Sci 2011;52:840–5.

53. Pedersen CJ, Huang D, Shure MA, Rollins AM. Measurement of absolute flow velocity vector using dual-angle, delay-encoded Doppler optical coherence tomography. Opt Lett 2007;32:506–8.

54. Srinivasan VJ, Sakadzic S, Gorczynska I, et al. Quantitative cerebral blood flow with optical coherence tomography. Opt Express [serial online] 2010;18:2477–94. Available at: http://www.opticsinfobase.org/oe/abstract.cfm?uri=oe-18-3-2477. Accessed December 10, 2013.

55. Baumann B, Potsaid B, Kraus MF, et al. Total retinal blood flow measurement with ultrahigh speed swept source/Fourier domain OCT. Biomed Opt Express [serial online] 2011;2:1539–52. Available at: http://www.opticsinfobase.org/boe/fulltext.cfm?uri=boe-2-6-1539&id=213997. Accessed December 10, 2013.

56. Zhi Z, Yin X, Dziennis S, et al. Optical microangiography of retina and choroid and measurement of total retinal blood flow in mice. Biomed Opt Express [serial online] 2012;3:2976–86. Available at: http://www.opticsinfobase.org/boe/fulltext.cfm?uri=boe-3-11-2976&id=244697. Accessed December 10, 2013.

57. Choi DH, Hiro-Oka H, Shimizu K, Ohbayashi K. Spectral domain optical coherence tomography of multi-MHz A-scan rates at 1310 nm range and real-time 4D-display up to 41 volumes/second. Biomed Opt Express [serial online] 2012; 3:3067–86. Available at: http://www.opticsinfobase.org/boe/fulltext.cfm?uri=boe-3-12-3067&id=244867. Accessed December 10, 2013.

58. Klein T, Wieser W, André R, et al. Multi-MHz FDML OCT: snapshot retinal imaging at 6.7 million axial-scans per second. In: Izatt JA, Fujimoto JG, Tuchin VV, eds. Proc SPIE 8213: Optical Coherence Tomography and Coherence Domain Optical Methods in Biomedicine XVI. San Francisco, CA: SPIE; 2012:82131E.

59. Potsaid B, Jayaraman V, Fujimoto JG, et al. MEMS tunable VCSEL light source for ultrahigh speed 60kHz-1MHz axial scan rate and long range centimeter class OCT imaging. In: Izatt JA, Fujimoto JG, Tuchin VV, eds. Proc. SPIE 8213: Optical Coherence Tomography and Coherence Domain Optical Methods in Biomedicine XVI. San Francisco, CA: SPIE; 2012:82130M.

Footnotes and Financial Disclosures

[1] Casey Eye Institute, Oregon Health & Science University, Portland, Oregon.

[2] Department of Electrical Engineering & Computer Science, Massachusetts Institute of Technology, Cambridge, Massachusetts.

[3] Advanced Imaging Group, Thorlabs, Inc, Newton, New Jersey.

[4] Pattern Recognition Lab and School of Advanced Optical Technologies, University Erlangen-Nuremberg, Erlangen, Germany.

Both authors Y.J. and S.T.B. contributed equally to this work.

Abbreviations and Acronyms:

AMD = age-related macular degeneration; **BM** = Bruch's membrane; **CNV** = choroidal neovascularization; **FA** = fluorescein angiography; **FAZ** = fovea avascular zone; **ICGA** = indocyanine green angiography; **OCT** = optical coherence tomography; **OPL** = outer plexiform layer; **PED** = pigment epithelial detachment; **RPE** = retinal pigment epithelial; **SSADA** = split-spectrum amplitude-decorrelation angiography; **3D** = 3-dimensional

Correspondence:

David Huang, MD, PhD, Casey Eye Institute, Oregon Health & Science University, 3375 SW Terwilliger Blvd., Portland, OR 97239-4197. E-mail: davidhuang@alum.mit.edu.